# Bone stress in runners with tibial stress fracture

Stacey A. Meardon [a,*], John D. Willson [a], Samantha R. Gries [b], Thomas W. Kernozek [b], Timothy R. Derrick [c]

[a] 2410 Health Sciences Building, Department of Physical Therapy, East Carolina University, Greenville, NC 27834, United States
[b] 1300 Badger Street, Health Professions Department, Physical Therapy Program, University of Wisconsin—La Crosse, La Crosse, WI 54601, United States
[c] 249 Barbara E. Forker Building, Department of Kinesiology, Iowa State University, Ames, IA 50011, United States

## ARTICLE INFO

## ABSTRACT

*Background:* Combinations of smaller bone geometry and greater applied loads may contribute to tibial stress fracture. We examined tibial bone stress, accounting for geometry and applied loads, in runners with stress fracture.

*Methods:* 23 runners with a history of tibial stress fracture & 23 matched controls ran over a force platform while 3-D kinematic and kinetic data were collected. An elliptical model of the distal 1/3 tibia cross section was used to estimate stress at 4 locations (anterior, posterior, medial and lateral). Inner and outer radii for the model were obtained from 2 planar x-ray images. Bone stress differences were assessed using two-factor ANOVA ($\alpha = 0.05$). Key contributors to observed stress differences between groups were examined using stepwise regression.

*Findings:* Runners with tibial stress fracture experienced greater anterior tension and posterior compression at the distal tibia. Location, but not group, differences in shear stress were observed. Stepwise regression revealed that anterior–posterior outer diameter of the tibia and the sagittal plane bending moment explained >80% of the variance in anterior and posterior bone stress.

*Interpretation:* Runners with tibial stress fracture displayed greater stress anteriorly and posteriorly at the distal tibia. Elevated tibial stress was associated with smaller bone geometry and greater bending moments about the medial–lateral axis of the tibia. Future research needs to identify key running mechanics associated with the sagittal plane bending moment at the distal tibia as well as to identify ways to improve bone geometry in runners in order to better guide preventative and rehabilitative efforts.

© 2015 Elsevier Ltd. All rights reserved.

## 1. Introduction

Running has become a popular means of exercise and, despite the numerous reported health benefits, runners are placed at risk for musculoskeletal injury. Stress fracture, one of the most serious musculoskeletal injuries that runners experience, accounts for 6–20% of all injuries in track and field athletes (Snyder et al., 2006). Distance runners are at increased risk for stress fracture due to the high impact and repetitive loads (Warden et al., 2006). The most common location of stress fracture is the tibia, where 19–54% of stress fractures are reported to occur (Iwamoto and Takeda, 2003; Snyder et al., 2006). Stress fractures in athletes are also the most prevalent between the ages of 15 and 24 years, at a time when bone quality should be enhanced (Ashe and Davis, 2005; Snyder et al., 2006). Therefore, an understanding of the potential etiology of stress fracture in runners is needed.

Repetitive mechanical loading of bone results in cumulative bone strain leading to bone damage and stress fracture if net bone damage chronically exceeds bone repair (Warden et al., 2006). A recent systematic review of the tibial stress fracture literature examined the relationship between the vertical ground reaction and stress fracture. This meta-analysis suggested that the vertical ground reaction forces during running were not greater in runners with stress fracture; however, average and instantaneous vertical loading rates associated with the impact peak during the stance phase did tend to be greater in those individuals with a history of stress fracture (Zadpoor and Nikooyan, 2011). Other measures of external load, including the peak free moment (Pohl et al., 2008) and the direction of the mediolateral ground reaction force relative to vertical have also been linked to tibial stress fracture (Creaby and Dixon, 2008). Taken as a whole, this line of evidence suggests that runners with tibial stress fracture display unique ground reaction force profiles, when compared to control runners, which may contribute to injury.

In addition to applied forces, bone structural properties influence stress. According to Crossley et al. and Franklyn et al., the cross sectional area (CSA) of the tibial cortex is less in male athletes with a history of tibial stress injury than uninjured male athletes (Crossley et al., 1999; Franklyn et al., 2008). Popp et al. and Schnackenburg et al. reported similar findings in female runners (Popp et al., 2009; Schnackenburg et al., 2011). Franklyn et al. also indicated geometric measures related to bone strength, specifically the second moment of area and section modulus in

* Corresponding author at: 2410D Health Sciences Building, East Carolina University, Greenville, NC 27858-4353, United States.
E-mail address: meardons@ecu.edu (S.A. Meardon).

male athletes and the section modulus in female athletes, were less in athletes with tibial stress injury (Franklyn et al., 2008). Reduced cortical bone parameters, similar to those reported in runners with stress fracture, will contribute to greater stress magnitude during running even if similar loads are applied. Given that runners with tibial stress fracture commonly display elevated loads and tend to have smaller tibiae, one would expect bone stress during running to be greater in runners with stress fracture compared to controls.

To date, no studies have simultaneously examined the components of bone stress, applied loads and bone geometry, in runners with a history of stress fracture. Moreover, external loads that have been examined to date neglect the influence of muscle forces and therefore may not fully represent the loading environment (Scott and Winter, 1990). The use of a musculoskeletal model that is scaled to individual bone geometry to estimate bone stress during running will improve our current knowledge of stress fracture in runners and allow researchers to better understand how running mechanics and bone geometry interact. Therefore, this study's primary purpose was to use subject-specific musculoskeletal modeling to examine differences in the bone stress in runners with and without a history of tibial stress fracture. We hypothesized that tibial bone stress would be elevated in runners with a history of tibial stress fracture when compared to controls. In addition, we sought to identify key bone geometries and applied loads that best predicted bone stress.

## 2. Methods

### 2.1. Subjects

This study received approval from the University Institutional Review Board. Prior to study participation, all subjects gave their written informed consent. A priori sample size was calculated, using G*Power Version 3.1.9.2, based on the stress values previously reported at the anterior and posterior tibia. The values from these locations were used since they are common locations of tibial stress fracture in runners (Nattiv et al., 2013). An alpha level of 0.05 with 80% power and a difference of 15% were used in our sample size calculations. This magnitude of difference has been considered to be clinically relevant based on previous running injury studies (Milner et al., 2007). Given these specifications, a minimum of 23 runners with and without a history of stress fracture were needed to reject the null hypothesis that these groups did not differ in the magnitude of anterior tension; 15 runners in each group were needed to reject the null hypothesis that the groups did not differ in posterior compression.

Twenty-three runners with a history of tibial stress fracture (SF) and 23 matched controls with no history of stress fracture (NSF) participated in this study. The NSF controls were matched to SF subjects based on gender, age, weekly mileage and self-reported 5 k race time (Table 1). Groups did not differ in menstrual history or contraceptive use (Table 1). Tibial stress fracture history was confirmed radiologically by

**Table 1**
Subject demographics. Means and standard deviations in parentheses are presented where appropriate. No significant differences on these variables were observed between groups (p > 0.05). SF indicates runners with a history of stress fracture and NSF indicates runners with no history of stress fracture.

| | Subject demographics | |
|---|---|---|
| | SF | NSF |
| Sex | 6 males, 17 females | 6 males, 17 females |
| Age (years) | 23.5 (6.0) | 23.7 (3.7) |
| Weekly mileage (km) | 29.3 (17.3) | 28.6 (17.0) |
| 5 k race time (min) | 21.8 (3.1) | 20.9 (5.2) |
| Height (m) | 1.71 (0.97) | 1.69 (0.99) |
| Mass (kg) | 64.49 (9.46) | 65.6 (12.4) |
| History of menstrual disturbance | 11 females | 10 females |
| History of contraceptive use | 9 females | 7 females |

a physician upon entry to the study. In order to participate in the study, subjects were required to be between the ages of 18 and 45, average at least 10 miles per week running, and currently running at least 50% of their pre-injury weekly mileage. Subjects were excluded from participation if they had a history of surgery on the study limb, impaired ability to run due to present pain or injury, or current pregnancy.

### 2.2. Procedure

Subjects underwent both sagittal and frontal plane X-ray of the tibia and completed an injury history questionnaire. Participant anthropometrics were also obtained for use in a musculoskeletal model: height, weight, thigh length, shank length, malleolar height, thigh circumference, calf circumference, foot length and breadth and malleolar width. Next, 32 spherical markers were applied to 8 segments of the body (thorax, pelvis and bilateral thigh, shank and foot) for 3 dimensional (3D) motion analysis during running. Anatomic markers were placed on the acromion, iliac crest, greater trochanters, medial and lateral femoral condyles, medial and lateral tibial plateau, medial and lateral malleoli, the 1st and 5th metatarsal heads and the tip of the shoe. Prior to dynamic running trials, a static calibration trial was collected for the estimation of joint centers and the anatomical markers were removed. Kinetic and kinematic data were collected through the use of a synchronized force platform (Model 4080, Bertec Corporation, Columbus, OH, 1200 Hz) with an eight-camera motion capture system (Motion Analysis, Centennial, CO, 120 Hz). Footwear was standardized for all subjects (New Balance 625 running shoes, Boston, MA USA).

For the motion trials, subjects ran across a 25 m runway over a force platform at a velocity corresponding to 3.7 m/s. The anterior–posterior coordinate of the sacral marker was used to monitor this running velocity and allowing feedback to be provided immediately following each trial. Participants performed a minimum of 10 warm up trials prior to data collection to ensure their natural gait. Additional practice was allowed as needed. Next, 10 running trials were recorded where the participant was running at the appropriate velocity with the study limb naturally making contact with the force platform. For the TSF group, the study limb was considered the limb that had previously sustained a stress fracture. The study limb of the matched controls were chosen based on limb dominance; if the study limb of a TSF runner was his or her dominant limb, the study limb for the matched control was the dominant limb and vice versa. Trials were repeated when the researcher observed the subject targeting the force platform, when running speed velocity fell outside the designated range, or when the subject did not strike the force platform with their entire foot.

### 2.3. Data analysis

Multiple steps were analyzed in order to calculate the stress at the tibia (Fig. 1). First, motion capture data, using a cubic spline technique, were interpolated to 1200 Hz to match kinetic data. Joint centers were approximated through the capture of static neutral standing trials. Three-dimensional Cardan segment and joint angles were then calculated with a flexion/extension, abduction/adduction, internal/external rotation sequence. Segment masses, center of mass location, and moments of inertia were estimated using anthropometric measurements (Vaughan et al., 1992). These estimates, in combination with 3D kinetic and kinematic data, were used to calculate reaction forces and net joint moments at the ankle, knee, and hip joints using inverse dynamics. Individual joint forces and moments were filtered according to the frequency content of the distal vertical reaction force (Edwards et al., 2011) using a 4th order low-pass Butterworth filter. The joint reaction force data were smoothed at the 98th percentile frequency of the distal vertical reaction force and the joint moment data were smoothed at the 95th percentile. An individually scaled musculoskeletal model was generated with the use of custom software to estimate length and velocity adjusted maximum muscle forces, muscle moment arms, and
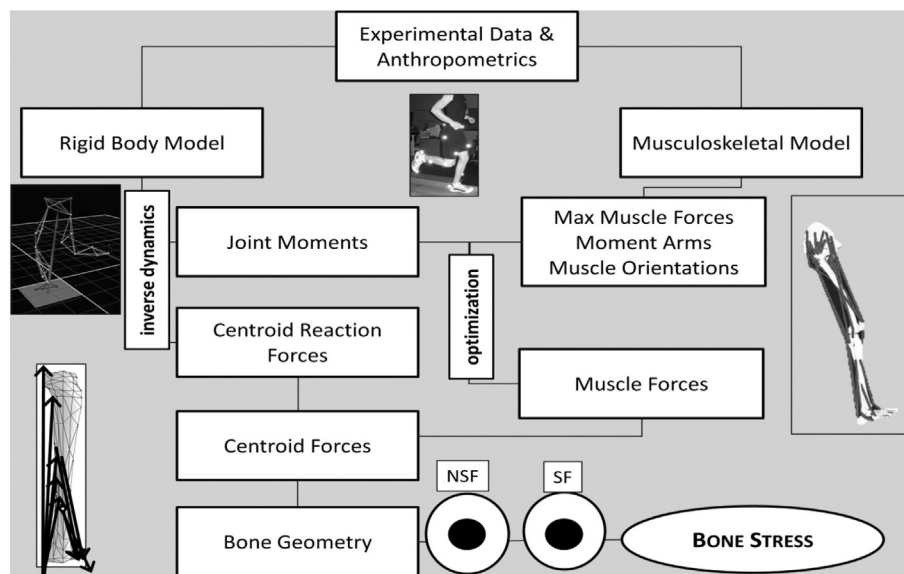
**Fig. 1.** Methods used in calculating bone stress.

muscle orientations of 44 lower extremity muscles (Arnold et al., 2010) during the stance phase of each running cycle. Static optimization, with a cost function minimizing the sum of squared muscle stresses, was used to estimate dynamic muscle forces during each trial (Glitsch and Baumann, 1997). The modeled muscle forces were constrained to match sagittal and frontal plane hip and sagittal plane knee and ankle moments from inverse dynamics. The resultant muscle forces, muscle moment arms, and muscle orientations were exported for later use in bone stress estimates.

X-ray images were viewed using public domain IrfanView software (irfanview.com) and converted to jpg file format for processing. From the x-rays, each subject's tibial length was measured from the tibial plateau to the talocrural joint line between the malleoli (Fig. 3a). Measurements of the anterior–posterior and medial–lateral tibial inner medullary cavity ($AP_i$ and $ML_i$, respectively) and outer periosteum ($AP_o$ and $ML_o$, respectively) diameters were then taken at a point corresponding to 67% of the length from the tibial plateau for entry into a bone model (Fig. 2b and c). An object of known length placed in the x-ray field of view allowed for the scaling of these measurements. Each of the measurements was performed by a single examiner (ICC = 0.97–0.99). AP and ML tibial inner and outer diameters were

used to scale an elliptical model of the tibia and to estimate the tibial cross sectional area (CSA), anterior–posterior moment of inertia ($I_{AP}$), and medial–lateral moment of inertia ($I_{ML}$). The following formulas were used to calculate the desired bone parameters (Milgrom, 1988):

$$CSA = \pi\left(\left(\frac{ML_o}{2}\right)\left(\frac{AP_0}{2}\right) - \left(\frac{ML_i}{2}\right)\left(\frac{AP_i}{2}\right)\right)$$

$$I_{ML} = \pi\left(\frac{ML_o}{2}\right)\left(\frac{AP_0}{2}\right)\left(\frac{\left(\frac{AP_o}{2}\right)^2}{4}\right) - \pi\left(\frac{ML_i}{2}\right)\left(\frac{AP_i}{2}\right)\left(\frac{\left(\frac{AP_i}{2}\right)^2}{4}\right)$$

$$I_{AP} = \pi\left(\frac{ML_o}{2}\right)\left(\frac{AP_0}{2}\right)\left(\frac{\left(\frac{ML_o}{2}\right)^2}{4}\right) - \pi\left(\frac{ML_i}{2}\right)\left(\frac{AP_i}{2}\right)\left(\frac{\left(\frac{ML_i}{2}\right)^2}{4}\right)$$

Each subject-specific tibia was modeled as a hollow ellipse. Stress ($\sigma$) was calculated at four locations (anterior, posterior, medial, and lateral) at the peripheral surface of the distal 1/3 of the tibia. This location is a common location for tibial stress fracture (Iwamoto and Takeda, 2003). The muscles crossing this location that were used in bone stress estimates included: soleus, gastrocnemius, tibialis anterior, tibialis
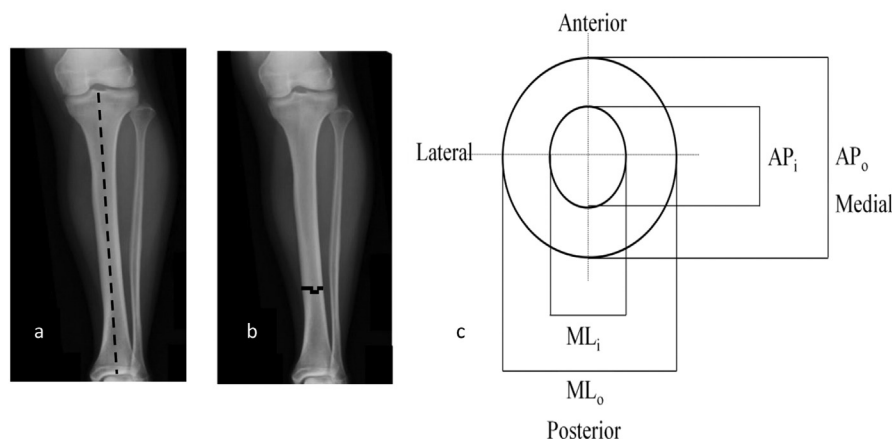


**Fig. 2.** a. Tibial length measurement (dashed line) taken from a sagittal plane x-ray. b. Tibial inner (solid lower line) and outer (dashed upper line) width measurements taken at a point corresponding to 67% of the length from the tibial plateau. Lines corresponding to inner and outer diameters were spaced for illustration purposes only. c. Cross sectional view of modeled tibia demonstrating the anterior–posterior (AP) and medial–lateral (ML) inner (i) and outer (o) bone dimensions used to calculate tibial CSA and $I_{AP}$ and $I_{ML}$. Bone diameters were taken from sagittal and frontal plane x-rays.

posterior, flexor digitorum, flexor hallucis longus, peroneal longus, peroneal brevis, peroneal tertius, and extensor digitorum longus.

Forces acting at the centroid were calculated by taking the vector sum of these muscle forces and the knee joint reaction force. Moments acting at the centroid were calculated by taking the cross product of each force and the point of application relative to the centroid position. For each of the four locations on the periphery of the bone, the stress due to the bending moment acting at the centroid and the stress due to longitudinal force were summed. As such, the following summary equations were used to calculate normal stress:

$$\sigma_{anterior} = \sigma(M_{ML}) + \sigma(F_{LONG})$$
$$\sigma_{lateral} = \sigma(-M_{AP}) + \sigma(F_{LONG})$$
$$\sigma_{posterior} = \sigma(-M_{ML}) + \sigma(F_{LONG})$$
$$\sigma_{medial} = \sigma(M_{AP}) + \sigma(F_{LONG}).$$

$F_{LONG}$ denotes the sum of the longitudinal tibial reaction force and the summed muscle forces acting longitudinally at the geometric center (centroid) of the tibia. $M_{ML}$ and $M_{AP}$ denote the sum of the bending moments due to the tibial reaction force and summed muscle moments acting about the respective medial–lateral and anterior–posterior axis of the centroid.

Shear stresses ($\tau$) were calculated by summing the shear stress due to torsional moments and centroid shear forces. At each location, the shear stress was calculated on the peripheral surface of the tibia using the following equations:

$$\tau_{anterior} = \tau(-M_{LONG}) + \tau(F_{ML})$$
$$\tau_{lateral} = \tau(M_{LONG}) + \tau(F_{AP})$$
$$\tau_{posterior} = \tau(M_{LONG}) + \tau(F_{ML})$$
$$\tau_{medial} = \tau(-M_{LONG}) + \tau(F_{AP}).$$

$F_{ML}$ denotes the sum of the medial–lateral tibia reaction force and the medial–lateral muscle forces acting about the centroid of interest. $F_{AP}$ denotes the sum of the anterior–posterior tibia reaction force and the anterior–posterior muscle forces acting about the centroid of interest. $M_{LONG}$ denotes the sum of the torsional moments due to the tibial reaction force and muscle moments acting about the longitudinal axis of the centroid.

### 2.4. Statistics

The average bending and shear stresses at the four tibial locations for each subject were analyzed in SPSS. A mixed model analysis of variance (ANOVA) was used to evaluate group differences in bone stress at 4 locations ($\alpha = 0.05$). Pairwise comparisons, with Bonferroni correction, were used to examine group differences at each location. Measured and calculated geometries were compared between groups with paired t-tests. Effect magnitude for all comparisons was analyzed through calculation of Cohen's d, with 0.2, 0.5, and 0.8 corresponding to small, medium, and large effect sizes respectively in order to demonstrate the magnitude of the between group differences (Cohen, 1992). In addition, stepwise linear regression was used to identify key bone geometry variables and internal bone forces and moments that best predicted bone stress at the locations that differed between groups. Criteria for the regression included the probability of F to enter being ≤0.05 and probability of F to remove ≥0.10. Co-linearity of bone geometry variables was assessed for each dependent variable prior to use in the stepwise regression in a hierarchical manner. Therefore, all bone geometry variables were entered into a regression model where these variables were then systematically removed, based on variance accounted for ($R^2$) and variance inflation factor (VIF), until the VIF fell below 10. Independent variables with least contribution to the variance of the dependent variable of interest were removed first. Non co-linear geometric predictors of observed stress differences between groups were then entered into a stepwise regression model with associated applied loads in order to determine the key predictors of bone stress.

## 3. Results

Ensemble group curves for normal and shear bone stress at the distal 1/3 of the tibia during the stance phase of running are illustrated in Figs. 3 and 4. Peak normal stresses tended to be tensile on the anterior and medial surfaces of the tibia and compressive on the posterior and lateral surfaces. Peak normal stress and shear stress tended to occur around 50% of stance phase (Figs. 3 and 4).

Statistical analysis indicated a group × location interaction for peak normal bone stress ($p = 0.012$). Pairwise comparisons revealed that the SF group demonstrated moderately greater anterior tensile stress (70.63 (SD 17.71) vs. 59.26 (SD 11.66) MPa; $p = 0.014$; $d = 0.76$) and moderately greater posterior compressive stress ($-101.77$ (SD 21.73) vs. $-89.77$ (SD 15.43) MPa; $p = 0.036$; $d = 0.64$) when compared to NSF. The mean group difference in anterior stress was 11.37 MPa and in posterior stress was 12.00 MPa, corresponding to 19% and 13% increase in stress when compared to the matched controls. The SF and NSF groups did not differ in peak tensile stress medially (23.88 (SD 11.64) vs. 26.23 (SD 10.53) MPa, $p = 0.477$, $d = 0.21$) or peak compression laterally ($-55.71$ (SD 16.46) vs. $-58.29$ (SD 11.91) MPa, $p = 0.545$, $d = 0.18$).

No group × location interaction or main effect for group was observed for peak shear stress ($p = 0.260$ and $p = 0.579$, respectively). However, shear stress did differ across locations ($p < 0.001$). Pairwise comparisons revealed that shear at the medial location (8.32 (SD 3.32 MPa)) was significantly greater than all other locations ($p < 0.001$ for all comparisons; $d = 0.44$–1.20). Shear at the posterior location (6.93 (SD 3.11 MPa)) was greater than the lateral location (4.70 (SD 3.73) MPa, $p < 0.001$, $d = 0.65$). Likewise, peak shear anteriorly (6.73 (SD 3.35 MPa)) exceeded peak shear laterally ($p < 0.001$, $d = 0.57$). Shear did not differ between the anterior and posterior tibia ($p = 0.338$, $d = 0.06$)

Measured and calculated bone geometries are displayed in Table 2. $ML_i$ tended to be moderately smaller in runners with SF ($p = 0.068$; $d = 0.55$) but all other bone parameters, with the exception of $ML_o$, were only slightly less in runners with stress fracture ($p > 0.05$; $d = 0.22$–0.38). After accounting for collinearity, anterior–posterior width of the outer tibia ($AP_o$) and area moment of inertia about the medial lateral axis of the tibia ($I_{ML}$) were the most significant geometric predictors of both anterior tensile stress ($R^2 = 0.27$) and posterior compressive stress ($R^2 = 0.26$) and were therefore included in the stepwise linear regression analysis to identify the key predictors of bone stress.

Stepwise linear regression was used to identify the key biomechanical predictors of bone stress values that differed between groups, anterior tension and posterior compression. Predictors entered into the model included $AP_o$, $I_{ML}$, and $F_{LONG}$ at peak stress and $M_{ML}$ at peak stress. Results suggested that $AP_o$ alone (Model 1) accounted for 27% of the variance in anterior tension and 26% of the variance in posterior compression. With both $AP_o$ and $M_{ML}$ occurring at peak stress (Model 2), 81% and 82% of the variance in anterior and posterior bone stress was accounted for, respectively (Table 3). Inclusion of $I_{ML}$ for both regression analyses resulted in significant collinearity (Model 3), indicating that this parameter provided little unique information to the prediction of peak stress.

## 4. Discussion

This study estimated the bone stress at the distal 1/3 of the tibia during running and compared the magnitudes of stress between runners with and without a previous tibial stress fracture. The results supported our hypothesis in that bone stresses were elevated in runners with a history of tibial stress fracture. Specifically, stresses were elevated anteriorly and posteriorly in the SF group when compared to the NSF group. Outer diameter of bone and internal moments acting on the bone together accounted over 80% of the variance in peak anterior and
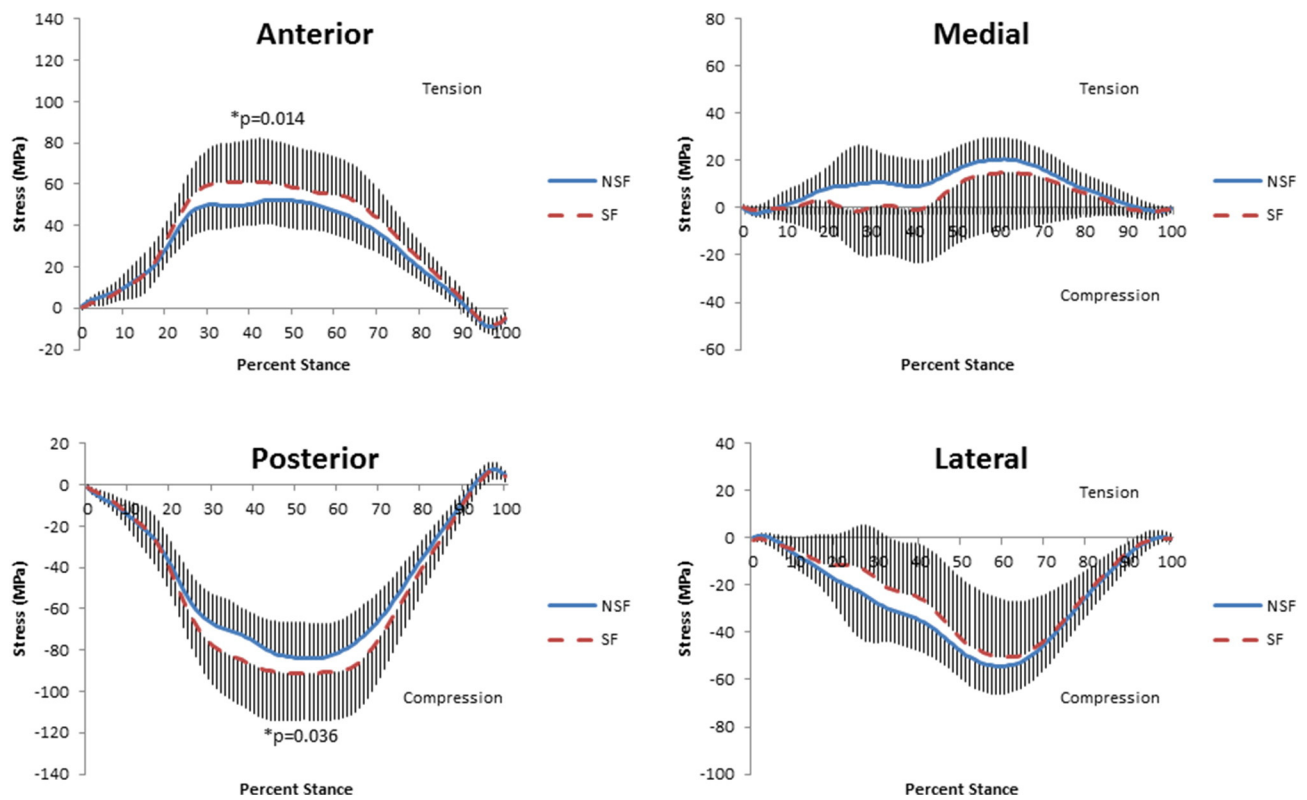
**Fig. 3.** Ensemble average and time normalized normal stress at 4 locations of the tibia at the distal 1/3 during the stance phase of running. Positive values indicate tension and negative indicate compression. A significant group difference in peak anterior and posterior stress was observed. Gray shaded areas represent standard deviation above or below the mean values (thick lines).
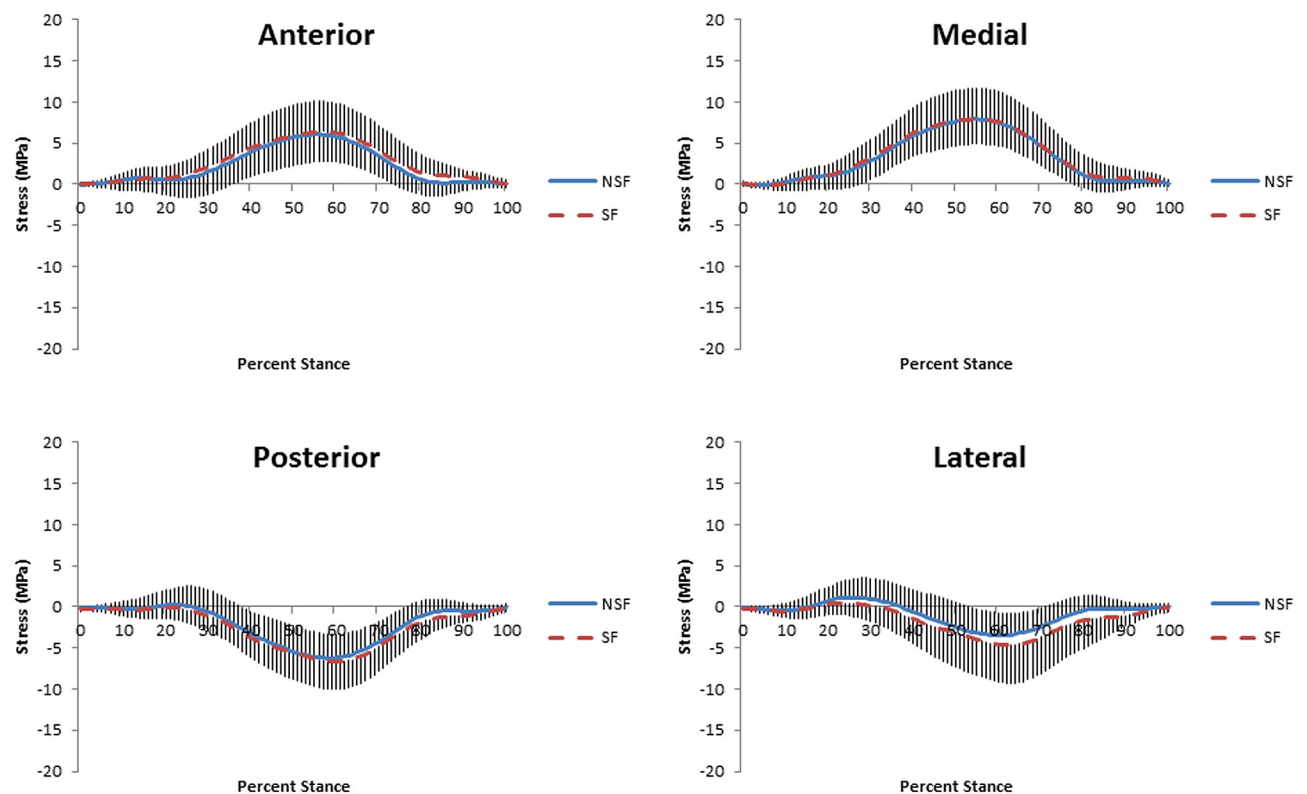


**Fig. 4.** Ensemble average and time normalized shear stress at 4 locations of the tibia at the distal 1/3 during the stance phase of running.

**Table 2**
Bone parameters measured or calculated in SF and NSF groups included inner and outer medial–lateral ($ML_o$) and anterior–posterior dimensions ($AP_o$), cross sectional area (CSA), anterior–posterior moment of inertia ($I_{AP}$), and medial–lateral moment of inertia ($I_{ML}$). SF indicates runners with a history of stress fracture and NSF indicates runners with no history of stress fracture.

| Bone parameters | | | | |
|---|---|---|---|---|
| | SF | NSF | Effect size (d) | p value |
| $AP_o$ (mm) | 24.64 (2.58) | 25.60 (2.93) | 0.380 | 0.245 |
| $ML_o$ (mm) | 22.77 (2.04) | 23.11 (1.98) | 0.169 | 0.578 |
| $AP_i$ (mm) | 9.27 (1.15) | 9.56 (1.27) | 0.239 | 0.422 |
| $ML_i$ (mm) | 9.76 (1.13) | 10.41 (1.21) | 0.555 | 0.068 |
| CSA ($mm^2$) | 370.85 (71.39) | 389.66 (87.97) | 0.235 | 0.430 |
| $I_{ap}$ ($mm^4$) | 14,383.50 (5588.47) | 15,654.29 (6094.23) | 0.217 | 0.465 |
| $I_{ml}$ ($mm^4$) | 17,079.72 (6799.55) | 19,753.75 (8785.59) | 0.340 | 0.255 |

posterior stresses, highlighting the importance of both bone geometry and gait mechanics in the evaluation of bone stress.

In order to substantiate our stress values, the stress observed at the medial aspect of the distal 1/3 tibia was converted to strain through the use of Hooke's Law and a Young's modulus of 20.9 GPa longitudinally and 12.3 GPa transversely (Hoffmeister et al., 2000) and compared to in vivo reports. Previous in vivo research, where strain gauges were mounted directly on the medial tibia during over ground running, reported medial tibia tensile strain values ranging from 394 to 1415 με and shear strains approximating 1444 με (Burr et al., 1996; Milgrom et al., 2000a,b, 2003, 2007). Across all subjects in this study, peak normal strain and peak shear strain at the medial tibia corresponded to 1198 (SD 594) με of tension and 676 (SD 270) με shear, respectively. A direct comparison between studies is difficult since bone strain values are influenced by the site of measurement as well as the shape of the tibia. Despite our simplification of the tibia by modeling it as a hollow ellipse, neglecting the irregular shape of the tibia, we attained reasonable estimates for peak normal stress medially compared to in vivo reports. However, shear stress observed in our investigation was relatively low. This is likely a consequence of using a homogenous model of the bone which has a symmetrical distribution of bone about the longitudinal axis. This symmetrical distribution may serve to minimize the effects of axial and bending loads in producing shear loading.

Using similar calculations mentioned in the previous paragraph, peak stresses at the anterior and posterior locations in this study corresponded to 3107 and −4582 με of anterior tension and posterior compression, respectively. These tensile and compressive strains fall within the reported microdamage threshold of 2000–4000 με, suggested by Frost, where microdamage appears to outpace repair (Frost, 1994). In agreement with Frost, Pattin et al. demonstrated a threshold of 2500 με for tension and 4000 με for compression before human cortical bone of the femur begins to show signs of microdamage accumulation (Pattin et al., 1996). In addition, Zioupos et al. demonstrated that

cortical bone of the femur accumulates microdamage with stresses ranging from 58 to 130 MPa (Zioupos et al., 1996). The anterior tensile stress in our SF participants (69.6 MPa) fell within the range of these potentially detrimental applied tensile stresses observed by Zioupos et al., and the stress in the NSF group fell within the low end this range (59.1 MPa). However, these values must be interpreted with caution. Our elliptical model is a simplification of the tibia, and future study incorporating subject-specific tibial shape appears warranted to confirm these findings. Further, it is important to note that this retrospective case–control study design reveals associations rather than causes. Loading characteristics observed may have been influenced by previous injury rather than causative in nature. However, evidence suggests that stress fracture recurrence is fairly common (Bennell et al., 2004; Newman et al., 2013; Sullivan et al., 1984); thus understanding post-injury loading seems warranted.

Tibial stress fractures in runners appear to be more common in certain locations. Nattiv et al. observed that the 18 of 20 tibial stress fractures in collegiate track and field and cross country runners occurred in the posteromedial aspect of the tibia (Nattiv et al., 2013). The remaining 2 stress fractures occurred in the anterior aspect of the tibia. Another study examining stress injury in general athletic populations reported stress fracture occurrence posteriorly in 75% of the cases, medially in 19% of the cases and anteriorly in 6% of the cases (Kijowski et al., 2012). The tendency for stress fracture to occur in the anterior and posterior tibia is seemingly consistent with the findings of this study. Our data indicated that the greatest tensile stress was observed anteriorly with moderately greater stress occurring in the stress fracture group. Also, the largest absolute stresses occurred posteriorly with runners who had a stress fracture displaying moderately greater posterior compressive stresses when compared to controls. High compressive stress in the posterior tibia is consistent with Sasimontonkul et al., who also observed the greatest force at the posterior tibia during midstance and suggested that this might be an explanation for the prevalence of tibial stress fractures in this location (Haris Phuah et al., 2010; Sasimontonkul et al., 2007). Previous work, using a similar standardized model of the tibia but with a different population, has also suggested that the largest stresses in the distal 1/3 of the tibia occurred posteriorly (Meardon and Derrick, 2014).

Based on these normal stress equations, stress on the anterior and posterior aspects of the tibia appears influenced by the longitudinal centroid reaction and muscle forces and the net moments acting about the ML axis of the tibia. The compressive force at the distal tibia, and subsequent anterior tensile force, has been suggested to be the result of force generated by the active ankle plantarflexors (Sasimontonkul et al., 2007). Moreover, the vertical ground reaction force, acting on a forwardly inclined tibia relative to the foot, contributes to the compression of the posterior distal tibia (Sasimontonkul et al., 2007). In a previous paper, we graphically illustrated that bending about the medial–lateral axis of the tibia is primarily dominated by the muscle forces and, to a

**Table 3**
Stepwise regression results for bone stress at sites that differed between SF and NSF are displayed. Correlation (R), variance accounted for ($R^2$), $R^2$ change with associated with each model are listed. Additionally, the F-statistic and p-value associated with model fit and the variation inflation factors (VIF) for each model variable are displayed.

| Stepwise regression results for anterior tension | | | | | | | |
|---|---|---|---|---|---|---|---|
| | Predictors | R | $R^2$ | $R^2$ change | F statistic | p-Value | VIF |
| Model 1 | $AP_o$ | 0.517 | 0.267 | 0.267 | 16.048 | <0.001 | 1.000 |
| Model 2 | $AP_o$, $M_{ML}$ | 0.906 | 0.820 | 0.553 | 98.267 | <0.001 | 1.795, 1.795 |
| Model 3 | $AP_o$, $M_{ML}$, $I_{ML}$ | 0.961 | 0.923 | 0.102 | 167.574 | <0.001 | 9.207,2.220, 11.198 |
| Model 4 | $AP_o$, $M_{ML}$, $I_{ML}$, $F_{LONG}$ | 0.970 | 0.940 | 0.018 | 161.869 | <0.001 | 9.210, 3.646, 11.214, 2.776 |
| Stepwise regression results for posterior compression | | | | | | | |
| Model 1 | $AP_o$ | 0.505 | 0.255 | 0.255 | 15.070 | <0.001 | 1.000 |
| Model 2 | $AP_o$, $M_{ML}$ | 0.905 | 0.818 | 0.563 | 96.790 | <0.001 | 1.795, 1.795 |
| Model 3 | $AP_o$, $M_{ML}$, $I_{ML}$ | 0.968 | 0.936 | 0.118 | 204.977 | <0.001 | 9.203, 2.216, 11.179 |

lesser extent, the reaction forces (Meardon and Derrick, 2014). It is therefore plausible that either, or both of these, may be elevated in runners with stress fracture. Stepwise regression analysis from the present study suggests that the sagittal plane bending moment about the medial–lateral axis of the tibia, once bone geometry is accounted for, is a key contributor to the magnitude of the anterior and posterior tibial stress. Previous research, along with this study, also shows that the greatest stress consistently occurs near midstance (Haris Phuah et al., 2010; Sasimontonkul et al., 2007; Scott and Winter, 1990). Thus, a better understanding of the kinetics and kinematics that contribute the sagittal plane bending of the tibia, and ultimately peak stress, during midstance appears warranted.

Previous findings appear to vary regarding differences in bone parameters between SF and NSF groups (Bennell et al., 2004; Franklyn et al., 2008; Milner et al., 2006; Popp et al., 2009; Snyder et al., 2006). No differences in bone parameters, estimated from x-ray, were observed in our study, but small to medium effect sizes were revealed which may become important with the repetitive loading associated with running long distances. Anterior–posterior outer tibial diameter, especially when combined with the sagittal plane bending moment, was a key contributor to bone stress on both the anterior and posterior surface of the tibia. These results highlight that both bone geometry and applied loads contribute to elevated bone stress in runners who have had a history of stress fracture. The clinical implications of these results are that exercises could be designed to enhance the structural characteristics of bone and efforts could be made to reduce stress during loading in order to reduce stress fracture odds. For instance, activities involving high forces delivered at a rapid rate with periods of rest inserted, as well as variable forces, could be prescribed to facilitate functional adaptation of bone to better resist applied loads (Honda et al., 2015; Warden et al., 2004; Weidauer et al., 2014). Additionally, runners with stress fracture may benefit from gait modification to reduce applied loads, in particular the sagittal plane bending moment acting at the tibia.

The results of this study need to be examined in light of several limitations not previously highlighted. Inherent error existed in our bone geometry measures since two dimensional images were used to estimate a three dimensional irregularly shaped tibia. However, this may not pose a significant problem since comparisons were made between groups of subjects within a specific study (Franklyn and Oakes, 2012). Nonetheless, comparisons of our data to other studies may be limited. Bone density, which in addition to bone geometry influences fracture resistance (Warden et al., 2005), was not examined in our subjects. Future models should evaluate the effects of bone density on modeled stresses and consider the addition of bone density accordingly. Static lower limb alignment, which varies among individuals, was not considered in this study. Lower limb alignment influences the mechanical axis between the hip and ankle centers of rotation, hence the kinetics data from the force plates during locomotion (Barrios et al., 2009; Mootanah et al., 2014). Although previous studies have not found an association between the mechanical axis of the tibia and frontal plane joint moments of the lower extremity during running (Willy et al., 2012), the relationship between the tibial mechanical axis and stress values should be examined. Areas of future study should examine identified risk factors (e.g. menstrual history, contraceptive use, static tibial alignment, bone density, activity history, fitness measures, bone geometry, gait mechanics), concurrently, in order to obtain a complete understanding of injury risk.

## 5. Conclusion

Our study demonstrates increased anterior and, to a lesser extent, posterior stress at the distal tibia in runners with a history of tibial stress fracture as compared to runners without a history of fracture during running. Bone geometry, in particular the outer anterior–posterior tibial measurement, partially contributed to elevated bone stress observed in runners with stress fracture. A better understanding of midstance running mechanics that contribute to elevated bone stress at the tibia during running will allow for improved prevention and rehabilitation of tibial stress fractures, a common running injury.

## Conflicts of interest

None.

## References

Arnold, E.M., Ward, S.R., Lieber, R.L., Delp, S.L., 2010. A model of the lower limb for analysis of human movement. Ann. Biomed. Eng. 38, 269–279.

Ashe, M.C., Davis, J.C., 2005. Bone health across the lifespan: implications for physical therapy practice. J. Women's Health Phys. Ther. 29, 13–18.

Barrios, J.A., Higginson, J.S., Royer, T.D., Davis, I.S., 2009. Static and dynamic correlates of the knee adduction moment in healthy knees ranging from normal to varus-aligned. Clin. Biomech. 24, 850–854.

Bennell, K., Crossley, K., Jayarajan, J., et al., 2004. Ground reaction forces and bone parameters in females with tibial stress fracture. Med. Sci. Sports Exerc. 36, 397–404.

Burr, D.B., Milgrom, C., Fyhrie, D., et al., 1996. In vivo measurement of human tibial strains during vigorous activity. Bone 18, 405–410.

Cohen, J., 1992. A power primer. Psychol. Bull. 112, 155–159.

Creaby, M.W., Dixon, S.J., 2008. External frontal plane loads may be associated with tibial stress fracture. Med. Sci. Sports Exerc. 40, 1669–1674.

Crossley, K., Bennell, K., Wrigley, T., Oakes, B.W., 1999. Ground reaction forces, bone characteristics, and tibial stress fracture in male runners. Med. Sci. Sports Exerc. 31, 1088–1093.

Edwards, W.B., Troy, K.L., Derrick, T.R., 2011. On the filtering of intersegmental loads during running. Gait Posture 34, 435–438.

Franklyn, M., Oakes, B., 2012. Tibial stress injuries: aetiology, classification, biomechanics and the failure of bone. An International Perspective on Topics in Sports Medicine and Sports Injury, pp. 509–534.

Franklyn, M., Oakes, B., Field, B., Wells, P., Morgan, D., 2008. Section modulus is the optimum geometric predictor for stress fractures and medial tibial stress syndrome in both male and female athletes. Am. J. Sports Med. 36, 1179–1189.

Frost, 1994. Wolff's Law and bone's structural adaptations to mechanical usage: an overview for clinicians. Angle Orthod. 64 (175), 175–188.

Glitsch, U., Baumann, W., 1997. The three-dimensional determination of internal loads in the lower extremity. J. Biomech. 30, 1123–1131.

Haris Phuah, A., Schache, A.G., Crossley, K.M., Wrigley, T.V., Creaby, M.W., 2010. Sagittal plane bending moments acting on the lower leg during running. Gait Posture 31, 218–222.

Hoffmeister, B., Smith, S., Handley, S., Rho, J., 2000. Anisotropy of Young's modulus of human tibial cortical bone. Med. Biol. Eng. Comput. 38, 333–338.

Honda, A., Matsumoto, M., Kato, T., Umemura, Y., 2015. Exercise characteristics influence femoral cross-sectional geometry: a magnetic resonance imaging study in elite female athletes. Osteoporos. Int. 26, 1093–1098.

Iwamoto, J., Takeda, T., 2003. Stress fractures in athletes: review of 196 cases. J. Orthop. Sci. 8, 273–278.

Kijowski, R., Choi, J., Shinki, K., Del Rio, A.M., De Smet, A., 2012. Validation of MRI classification system for tibial stress injuries. Am. J. Roentgenol. 198, 878–884.

Meardon, S.A., Derrick, T.R., 2014. Effect of step width manipulation on tibial stress during running. J. Biomech. 47, 2738–2744.

Milgrom, C., Giladi, M., Simkin, A., et al., 1988. An analysis of the biomechanical mechanism of tibial stress fractures among Israeli infantry recruits: a prospective study. Clin. Orthop. Relat. Res. 231, 216–221.

Milgrom, C., Finestone, A., Levi, Y., et al., 2000a. Do high impact exercises produce higher tibial strains than running? Br. J. Sports Med. 34, 195–199.

Milgrom, C., Finestone, A., Segev, S., Olin, C., Arndt, T., Ekenman, I., 2003. Are overground or treadmill runners more likely to sustain tibial stress fracture? Br. J. Sports Med. 37, 160–163.

Milgrom, C., Finestone, A., Simkin, A., et al., 2000b. In vivo strain measurements to evaluate the strengthening potential of exercises on the tibial bone. J. Bone Joint Surg. (Br.) 82, 591–594.

Milgrom, C., Radeva-Petrova, D.R., Finestone, A., et al., 2007. The effect of muscle fatigue on in vivo tibial strains. J. Biomech. 40, 845–850.

Milner, C.E., Ferber, R., Pollard, C.D., Hamill, J., Davis, I.S., 2006. Biomechanical factors associated with tibial stress fracture in female runners. Med. Sci. Sports Exerc. 38, 323–328.

Milner, C.E., Hamill, J., Davis, I., 2007. Are knee mechanics during early stance related to tibial stress fracture in runners? Clin. Biomech. 22, 697–703.

Mootanah, R., Imhauser, C.W., Reisse, F., et al., 2014. Development and validation of a computational model of the knee joint for the evaluation of surgical treatments for osteoarthritis. Comput. Methods Biomech. Biomed. Engin. 17, 1502–1517.

Nattiv, A., Kennedy, G., Barrack, M.T., et al., 2013. Correlation of MRI grading of bone stress injuries with clinical risk factors and return to play: a 5-year prospective study in collegiate track and field athletes. Am. J. Sports Med. 41, 1930–1941.

Newman, P., Witchalls, J., Waddington, G., Adams, R., 2013. Risk factors associated with medial tibial stress syndrome in runners: a systematic review and meta-analysis. Open Access J. Sports Med. 4, 229–241.

Pattin, C.A., Daler, W.E., Carter, D.R., 1996. Cyclic mechanical property degradation during fatigue loading of cortical bone. J. Biomech. 29, 69–79.

Pohl, M.B., Mullineaux, D.R., Milner, C.E., Hamill, J., Davis, I.S., 2008. Biomechanical predictors of retrospective tibial stress fractures in runners. J. Biomech. 41, 1160–1165.

Popp, K.L., Hughes, J.M., Smock, A.J., et al., 2009. Bone geometry, strength, and muscle size in runners with a history of stress fracture. Med. Sci. Sports Exerc. 41, 2145–2150.

Sasimontonkul, S., Bay, B.K., Pavol, M.J., 2007. Bone contact forces on the distal tibia during the stance phase of running. J. Biomech. 40, 3503–3509.

Schnackenburg, K.E., Macdonald, H.M., Ferber, R., Wiley, J.P., Boyd, S.K., 2011. Bone quality and muscle strength in female athletes with lower limb stress fractures. Med. Sci. Sports Exerc. 43, 2110–2119.

Scott, S.H., Winter, D.A., 1990. Internal forces of chronic running injury sites. Med. Sci. Sports Exerc. 22, 357–369.

Snyder, R.A., Koester, M.C., Dunn, W.R., 2006. Epidemiology of stress fractures. Clin. Sports Med. 25, 37–52.

Sullivan, D., Warren, R.F., Pavlov, H., Kelman, G., 1984. Stress fractures in 51 runners. Clin. Orthop. Relat. Res. 187, 188–192.

Vaughan, C.L., Davis, B.L., O'connor, J.C., 1992. Dynamics of Human Gait. Human Kinetics, Champaign, IL.

Warden, S.J., Burr, D.B., Brukner, P.D., 2006. Stress fractures: pathophysiology, epidemiology, and risk factors. Curr. Osteoporos. Rep. 4, 103–109.

Warden, S.J., Fuchs, R.K., Turner, C.H., 2004. Steps for targeting exercise towards the skeleton to increase bone strength. Eura. Medicophys. 40, 223–232.

Warden, S.J., Hurst, J.A., Sanders, M.S., Turner, C.H., Burr, D.B., Li, J., 2005. Bone adaptation to a mechanical loading program significantly increases skeletal fatigue resistance. J. Bone Miner. Res. 20, 809–816.

Weidauer, L., Minett, M., Negus, C., et al., 2014. Odd-impact loading results in increased cortical area and moments of inertia in collegiate athletes. Eur. J. Appl. Physiol. 114, 1429–1438.

Willy, R.W., Manal, K.T., Witvrouw, E.E., Davis, I.S., 2012. Are mechanics different between male and female runners with patellofemoral pain? Med. Sci. Sports Exerc. 44, 2165–2171.

Zadpoor, A.A., Nikooyan, A.A., 2011. The relationship between lower-extremity stress fractures and the ground reaction force: a systematic review. Clin. Biomech. 26, 23–28.

Zioupos, P., Wang, X., Currey, J., 1996. The accumulation of fatigue microdamage in human cortical bone of two different ages in vitro. Clin. Biomech. 11, 365–375.